Structural Engineering and Mechanics, *Vol. 48, No. 1 (2013) 17-39*
DOI: http://dx.doi.org/10.12989/sem.2013.48.1.017

A smeared crack model for seismic failure analysis of concrete gravity dams considering fracture energy effects

Mohammad Amin Hariri-Ardebili*[1], Seyed Mahdi Seyed-Kolbadi[2] and Hasan Mirzabozorg[2]

[1]*Department of Civil, Environmental and Architectural Engineering, University of Colorado at Boulder, ECCE 168, UBC 80309-0428, Boulder, CO, USA*
[2]*Department of Civil Engineering, K. N. Toosi University of Technology, Vali-asr St., 15875-4416, Tehran, Iran*

(Received January 2, 2012, Revised July 30, 2013, Accepted September 18, 2013)

Abstract. In the present paper, a coaxial rotating smeared crack model is proposed for mass concrete in three-dimensional space. The model is capable of applying both the constant and variable shear transfer coefficients in the cracking process. The model considers an advanced yield function for concrete failure under both static and dynamic loadings and calculates cracking or crushing of concrete taking into account the fracture energy effects. The model was utilized on Koyna Dam using finite element technique. Dam-water and dam-foundation interactions were considered in dynamic analysis. The behavior of dam was studied for different shear transfer coefficients considering/neglecting fracture energy effects. The results were extracted at crest displacement and crack profile within the dam body. The results show the importance of both shear transfer coefficient and the fracture energy in seismic analysis of concrete dams under high hydrostatic pressure.

Keywords: concrete gravity dam; smeared crack model; shear transfer coefficient; fracture energy

1. Introduction

Many of structures such as buildings, bridges, dams, and nuclear power plants are constructed from either mass or reinforced concrete material. Investigation of the cracking mechanism of concrete structures under both static and dynamic loads is important for safety operation of existing structures during their service life. Complex models are required in order to capture the pre- and port cracking behavior of concrete mortar. Several researchers have introduced approaches in order to modeling the nonlinear behavior of concrete under time-varying loads. The methods based on continuum crack model, discrete crack model, interface crack approach and the method of constrains are some of the most favorite methods for numerically modeling of concrete material. Numerical methods such as finite element, finite difference, finite volume, extended finite element, and mesh free approaches are also common methods for simulation of structural systems and their behavior (Yu *et al.* 2008).

The discrete crack model requires monitoring the response and modifying topology of the mesh

*Corresponding author, Ph.D. Student, E-mail: mohammad.haririardebili@colorado.edu

http://www.techno-press.org/?journal=sem&subpage=8 ISSN: 1225-4568 (Print), 1598-6217 (Online)

corresponding to the current crack configurations at each state of loading. This approach explicitly represents the crack as a separation of nodes, which is a more realistic representation of the opened crack. This model is useful when the location and direction of the cracks are recognizable before loading the structure. The methods based on continuum crack model are divided into two major groups, i.e., damage mechanics and smeared crack approaches. In the smeared crack approach, cracks and joints are modeled in an average sense by appropriately modifying the material properties at the integration points of regular finite elements. Smeared cracks are convenient when the crack orientations are not known beforehand, because the formation of a crack involves no re-meshing or new degrees of freedom.

Some researchers applied continuum damage mechanics to investigate the concrete behavior among them Mirzabozorg *et al.* (2004), Labadi and Hannachi (2005), Grassl and Jirásek (2006), Cicekli *et al.* (2007), Voyiadjis *et al.* (2009), Al-Rub and Kim (2010), Xue and Yang (2013). Failure based on the smeared crack approach and classification of its branches studied by Malvar and Fourney (1990), Weihe *et al.* (1998), Moslera and Meschke (2004), Phama *et al.* (2006), Mirzabozorg *et al.* (2007), Suryanto *et al.* (2010), Broujerdian and Kazemi (2010), Heinrich and Waasy (2012).

Seismic failure analysis of concrete gravity dams, especially Koyna Dam, studied by several researchers. Bhattacharjee and Leger (1994) studied nonlinear response of Koyna Dam based on smeared crack approach and compared results with those obtained from laboratory test. Ghaemian and Ghobarah (1999) investigated the application of a two-dimensional smeared crack model for seismic assessment of gravity dams. Two-dimensional seismic fracture behavior of Koyna Dam was examined by Guanglun *et al.* (2000) using smeared crack model. Calayir and Karaton (2005) used fracture mechanics approach for seismic analysis of Koyna Dam using Lagrange-Lagrange formulation for the fluid-structure interaction. Mirzabozorg and Ghaemian (2005) used smeared crack model for crack analysis of gravity and arch dams. They used a simplified model for concrete failure and modeled the reservoir using the fluid finite elements. Lohrasbi and Attarnejad (2008) used fracture mechanics in conjunction with smeared crack and discrete crack models for analysis of concrete dams.

The specific fracture energy, G_f, as defined by the RILEM (RILEM TC-50 FMC 1985) is one of the most well-known, frequently measured and used fracture properties of concrete. While the simplicity in its definition and experiment has certainly contributed to its broad acceptance, the position of G_f in fracture mechanics of concrete is really cemented by its inherent relationship with the widely-accepted fictitious crack model (Duan *et al.* 2007). The area under the common tensile softening curve or the curve of cohesive stress and crack opening of a fictitious crack determines the specific fracture energy. The original intention of the RILEM definition of fracture energy as given in RILEM TC-50 FMC (1985) was that the material constant G_f, determined by the tensile softening curve as stated by the fictitious crack model, could also be measured from the load and load-point displacement curve of concrete. However, size effect on G_f typically measured from specimens less than 0.5m is overwhelming, and the phenomenon is possibly just as well-known as G_f itself. Both the application and validity of the fictitious crack model require a constant G_f as the tensile softening relationship together with G_f is treated as a fundamental material property for each element according to its dimensions. The accuracy of the results in smeared crack model would be compromised if the size effect on G_f and its effect on each element of model were not correctly implemented (Duan *et al.* 2003). Ayari and Saouma (1990), Saouma and Milner (1996), and Saouma and Morris (1998) presented detailed case studies and investigated different aspects of the fracture mechanics approach and its application on concrete dams. Ghrib and Tinawi (1995) used fracture energy in nonlinear seismic response of concrete gravity dams. Duan *et al.* (2007) studied size effects in concrete gravity dams considering appropriate fracture energy in numerical models. Hu and Duan (2004) investigated the effects of fracture process zone height on fracture energy of concrete.

In the present paper, a coaxial smeared crack model is introduced in 3D space and the importance of the size effect and its corresponding fracture energy is investigated for seismic failure analysis of a concrete gravity dam. An advanced three-parameter yield criterion is utilized in finite element formulation. The effect of reservoir water is considered for calculation of hydrodynamic pressure on the upstream face.

2. Modeling of concrete

The present model is able to simulate the behavior of the concrete material in various states as following: pre-softening behavior; fracture energy conservation; nonlinear behavior during the softening phase and finally crack closing/reopening behavior. The contribution of authors is to developing a three-dimensional coaxial rotating smeared crack model and implementing the fracture energy effects in the finite element model for dynamic analysis of concrete structures. Also the three-parameter Menetrey and Willam (1995) yield criterion is utilized for the first time in conjunction with rotating smeared crack for the concrete structures under the high hydrostatic pressure. The following sub-sections represent a brief review on general concepts of these stages.

2.1 Pre-softening phase

Generally, the relationship of the stress and strain vectors at the pre-softening phase is given by

$$\{\sigma\} = [D]_{elastic}\{\varepsilon\} \tag{1}$$

where $[D]_{elastic}$ is the elastic modulus matrix; $\{\sigma\}$ and $\{\varepsilon\}$ are the vectors of stress and strain components respectively. The modulus matrix in elastic condition can be defined for isotropic, orthotropic or anisotropic materials. However, in most cases the isotropic material is assumed for mass concrete at the pre-softening phase.

2.2 Softening phase

During the softening phase, the elastic stress-strain relationship is substituted with an anisotropic modulus matrix, which corresponds to the stiffness degradation level in the three principal directions. In the present study, the secant modulus stiffness approach, SMS, is unitized for the stiffness formulation in which the constitutive relation is defined in terms of total stresses and strains, shown in Fig. 1. In this figure, σ_n and ε_n are the total normal stress and strain on fracture plane, respectively. σ_0 and ε_0 are the apparent tensile strength and its corresponding strain, respectively. $\varepsilon_{\max}$ and ε_f are the maximum strain in stiffness formulation and the fracture strain, respectively. In addition, E, E^s and E^t are the elastic Young's modulus, softened Young's modulus in the direction normal to the fracture plane, and the tangent modulus, respectively. The stiffness modulus matrix based on the smeared crack propagation model is given in Eq. (2). It is noteworthy that the extracted modulus matrix is coaxial with the principal strains in the considered location within the cracked element. Details of the formulation and the utilized algorithm including

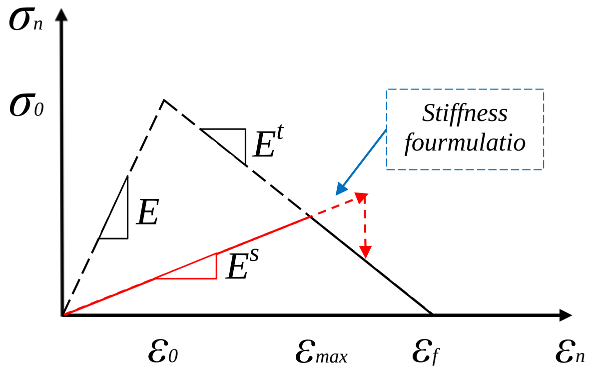

Fig. 1 SMS formulation of stiffness modulus matrix

unloading/reloading path and the residual strain in the closed cracks can be found in Mirzabozorg and Ghaemian (2005).

The total secant modulus matrix in local coordinates is given as

$$[D]_{crack}^{local} = \begin{bmatrix} \left[D^t\right]_{crack}^{local} & \mathbf{0} \\ \mathbf{0} & \left[D^r\right]_{crack}^{local} \end{bmatrix} \tag{2}$$

where

$$\left[D^t\right]_{crack}^{local} = \begin{bmatrix} D_{11} & D_{12} & D_{13} \\ & D_{22} & D_{23} \\ sym. & & D_{33} \end{bmatrix}, \quad \left[D^r\right]_{crack}^{local} = \begin{bmatrix} D_{44} & 0 & 0 \\ & D_{55} & 0 \\ sym. & & D_{66} \end{bmatrix} \tag{3}$$

Components of the abovementioned matrices are as follow

$$D_{11} = \frac{E}{\Gamma}\left(\eta_1 - \upsilon^2\eta_1\eta_2\eta_3\right), D_{22} = \frac{E}{\Gamma}\left(\eta_2 - \upsilon^2\eta_1\eta_2\eta_3\right), D_{33} = \frac{E}{\Gamma}\left(\eta_3 - \upsilon^2\eta_1\eta_2\eta_3\right)$$

$$D_{12} = \frac{E}{\Gamma}\left(\upsilon\eta_1\eta_2 + \upsilon^2\eta_1\eta_2\eta_3\right), D_{23} = \frac{E}{\Gamma}\left(\upsilon\eta_2\eta_3 + \upsilon^2\eta_1\eta_2\eta_3\right), D_{13} = \frac{E}{\Gamma}\left(\upsilon\eta_1\eta_3 + \upsilon^2\eta_1\eta_2\eta_3\right) \tag{4}$$

$$D_{44} = \beta_{12}G, D_{55} = \beta_{23}G, D_{66} = \beta_{13}G$$

where, η_1, η_2 and η_3 are the ratio of the softened Young's modulus in the three principal directions and the initial isotropic elastic modulus and β_{12}, β_{23} and β_{13} are shear transfer coefficients corresponding to the principal directions given as

$$\beta_{12} = \frac{1+\upsilon}{\Gamma}\left(\frac{\eta_1\varepsilon_1 - \eta_2\varepsilon_2}{\varepsilon_1 - \varepsilon_2} + \frac{\upsilon\eta_3\left(\eta_1 - \eta_2\right)\varepsilon_3}{\varepsilon_1 - \varepsilon_2} - \upsilon\eta_1\eta_2 - 2\upsilon^2\eta_1\eta_2\eta_3\right)$$

$$\beta_{23}=\frac{1+\upsilon}{\Gamma}\left(\frac{\eta_2\varepsilon_2-\eta_3\varepsilon_3}{\varepsilon_2-\varepsilon_3}+\frac{\upsilon\eta_1\left(\eta_2-\eta_3\right)\varepsilon_1}{\varepsilon_2-\varepsilon_3}-\upsilon\eta_2\eta_3-2\upsilon^2\eta_1\eta_2\eta_3\right)$$

$$\beta_{13}=\frac{1+\upsilon}{\Gamma}\left(\frac{\eta_1\varepsilon_1-\eta_3\varepsilon_3}{\varepsilon_1-\varepsilon_3}+\frac{\upsilon\eta_2\left(\eta_1-\eta_3\right)\varepsilon_2}{\varepsilon_1-\varepsilon_3}-\upsilon\eta_1\eta_3-2\upsilon^2\eta_1\eta_2\eta_3\right) \tag{5}$$

$$\Gamma=1-\upsilon^2\eta_1\eta_2-\upsilon^2\eta_2\eta_3-\upsilon^2\eta_1\eta_3-2\upsilon^3\eta_1\eta_2\eta_3$$

The constitutive matrix given in Eq. (2) is transformed to the global coordinate system as following

$$\left[D\right]_{crack}^{global}=\left[T\right]^T\left[D\right]_{crack}^{local}\left[T\right] \tag{6}$$

where, $[T]$ is the strain transformation matrix in three-dimensional space. Based on the maximum strain reached in each principal direction, the secant modulus matrix is determined. Increasing the normal strain in each principal direction leads to reduction of the corresponding softened Young's modulus. Finally, when the maximum strain reaches the fracture strain, the considered Gaussian point within the element in the corresponding direction is fully cracked and its contribution in the stiffness matrix of the element is eliminated. Based on Eq. (2) to Eq. (6), any change in principal strains or their directions in each Gaussian point leads to an update requirement of the global constitutive matrix, $\left[D\right]_{crack}^{global}$. In the proposed model, there is residual strain even when the crack is close. The shear retention factors are not zero and are determined based on the Eq. (5) in terms of principal strain and softened Yong's Modulus in each direction (Mirzabozorg and Ghaemian 2005). Satisfying the energy conservation principle in each Gaussian point leads to the fracture strain under static and dynamic loads

$$\varepsilon_f=\frac{2G_f}{\sigma_0 h_c},\quad \varepsilon'_f=\frac{2G'_f}{\sigma'_0 h_c} \tag{7}$$

where, h_c is the characteristic dimension of the considered Gaussian point and is assumed equal to the cubic root of the Gaussian point's volume contribution; σ_0 is the stress corresponding to the softening strain and G_f is the specific fracture energy. The primed quantities show the dynamic constitutive parameters. The strain-rate sensitivity of fracture energy is applied through a dynamic magnification factor, DMF_f, so that

$$G'_f=DMF_f G_f \tag{8}$$

2.3 Conservation of fracture energy

It should be noted that the fracture energies G_F, obtained by the work-of-fracture method, and G_f, obtained by the size effect method, are two different material characteristics (Einsfeld and Velasco 2006). Parameter G_F represents the area under the complete load-defection curve while G_f represents the area under the initial tangent of the softening curve and determines the maximum load of most concrete structures in practice. The area under the average stress-strain curve of a finite element that experiences cracking is defined in a way that the dissipated fracture energy stays independent of the element characteristics dimension. In order for the fracture energy to be conserved, the softening branch should be modified using the following relationship (Bazant 2002)

$$E^t = \frac{f_t'^2 E}{f_t'^2 - 2E G_f / h_c} \tag{9}$$

Fracture energy is the key parameter that is combined with elastic modulus and tensile strength to define the entire constitutive behavior of concrete in the nonlinear fracture mechanics models. Usually, the tensile strength beyond which a strain softening process is assumed to take place is determined from uniaxial or split cylinder tests and the fracture energy, G_f from wedge splitting tests (Briihwiler and Wittmann 1990).

2.4 Failure criterion

The strength of concrete under multi-axial stresses is a function of the state of stress and cannot be predicted by limitation of simple tensile, compressive and shearing stresses independently of each other. In the elasticity based models, a suitable failure criterion is incorporated for a complete description of the ultimate strength surface. Criteria such as yielding, load carrying capacity and initiation of cracking have been used to define failure (Babu *et al.* 2005). Many failure criterions have been proposed for brittle material as well as mass concrete. The most commonly used failure criteria are defined in stress space using some independent constant parameters varying from one to seven (Bigoni and Piccolroaz 2004). Generally using the higher-order failure criteria can leads to better results while it requires more experimental tests in order to determination of the material constant parameters. In the present study, an advanced three-parameter Menetrey and Willam (1995) failure criterion is used for initiation and propagation of cracks in mass concrete. This criterion was obtained by modifying the well-known Hoek and Brown criterion for rock masses. The criterion is different from the other formulations in its ability to handle physical changes like crack closure, and is not restricted to any particular shape of hardening/softening laws. In the general form this yield function can be expressed as follow

$$f(\xi,\rho,\theta) = \left[\sqrt{\frac{3}{2}}\frac{\rho}{f_c'}\right]^2 + m\left[\frac{\rho}{\sqrt{6}f_c'}r(\theta,e) + \frac{\xi}{\sqrt{3}f_c'}\right] - c = 0 \tag{10}$$

where (ξ, ρ, θ) are Heigh-Vestergaard coordinates; ξ is hydrostatic stress invariant, ρ is deviatory stress invariant, θ is deviatory polar angle. $r(\theta, e)$ is an elliptic function, e describes the shape of the deviatory trace. The failure surface has sharp corners if e = 0.5 and is fully circular around the hydrostatic axis if e = 1.0. The parameter m represents the frictional resistance of material, c is cohesion of material, and f'_c and f'_t are uniaxial compressive and tensile strength of concrete, respectively. The main parameters in the above equation are defined as follow

$$\begin{gathered} \xi = \frac{I_1}{\sqrt{3}}, \quad \rho = \sqrt{2J_2}, \quad \theta = \frac{1}{3}\cos^{-1}\left(\frac{3\sqrt{3}}{2}\frac{J_3}{J_2^{3/2}}\right) \\ I_1 = \sigma_{ii}, \quad J_2 = \frac{1}{2}S_{ij}S_{ji}, \quad J_3 = \frac{1}{3}S_{ij}S_{jk}S_{ki} \end{gathered} \tag{11}$$

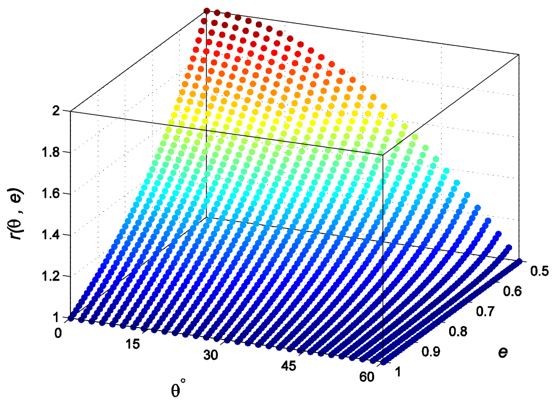

Fig. 2 Elliptic function of Menetrey and Willam (1995) failure criterion

in which, I_1 is the first invariant of the Cauchy stress tensor; J_2 and J_3 are the second and third invariants of the deviatory part of the Cauchy stress tensor; σ_{ii} is principal stress; S_{ij}, S_{ji}, S_{jk} and $S_{ki}$are deviatory stresses. In addition, the elliptic function (Fig. 2) and the frictional resistance of material are given as

$$r(\theta, e) = \frac{4\left(1-e^2\right)\cos^2\theta + \left(2e-1\right)^2}{2\left(1-e^2\right)\cos\theta + \left(2e-1\right)\left[4\left(1-e^2\right)\cos^2\theta + 5e^2 - 4e\right]^{1/2}} \tag{12}$$

$$m = \frac{\sqrt{3}e}{e+1}\frac{f_c'^2 - f_t'^2}{f_c'\, f_t'} \tag{13}$$

3. Verification of proposed model

3.1 Three-point bending test of a notched beam

A simple notched beam under three-point bending test is used for verifying of the proposed model. Fig. 3(a) shows the general view of the three-point bending test based on Malvar and Warren (1988). The material properties are as follow: E=21.7GPa, υ=0.2, f'_t=2.4MPa, f'_c=29.0MPa, and G_f=35N/m. Fig. 3(b) compares the load versus load-point deflection curves resulted from Malvar and Warren (1988) experimental test and the finite element model based on smeared crack model with variable shear transfer coefficient in the present study, Hariri-Ardebili *et al.* As seen, there is good agreement between the numerical model and the experimental test through all loading stages: elastic, hardening, and softening; which demonstrates the soundness of the present algorithm. For the comparison purpose, the result of the elastic-plastic-damage model proposed by Voyiadjis and Taqieddin (2009) also presented in this figure. As seen, both the numerical models have close estimation of the experimental test before the softening point; however, Hariri-Ardebili *et al.* model provides closer result. Generally in the softening phase, Voyiadjis and Taqieddin (2009) model estimates higher deflection than the experimental test for a

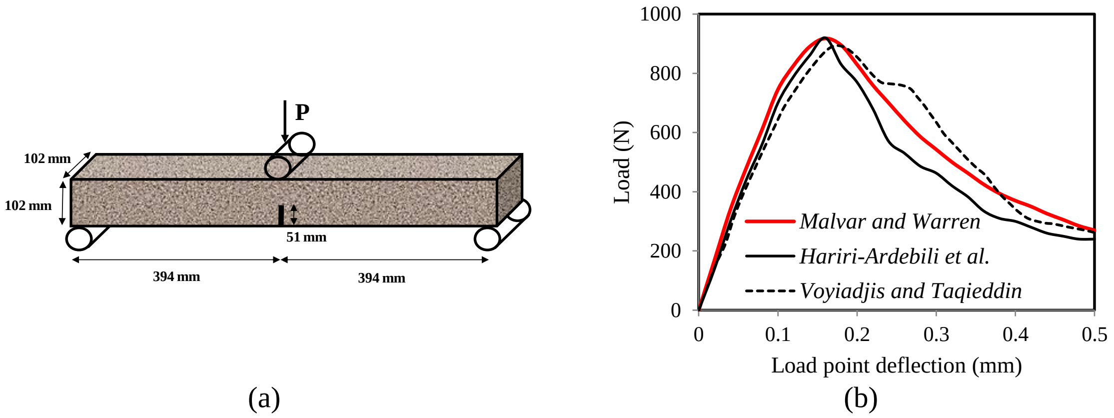

Fig. 3 (a) Geometry of single-edge-notched beam subjected to three point bending test; (b) Load versus load-point deflection

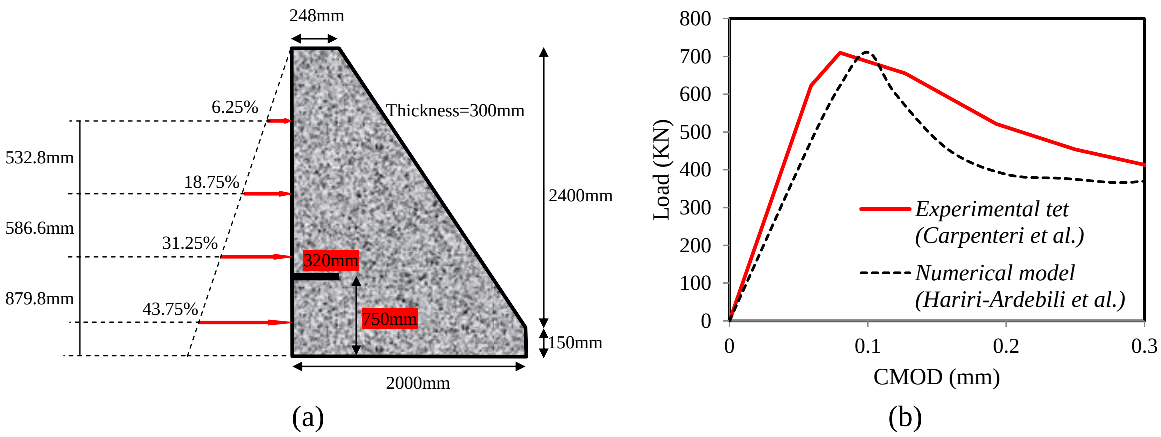

Fig. 4 (a) Experimental monolith the scaled typical concrete gravity dam; (b) Load versus CMOD of the notch for experimental test and numerical model

certain applied load, while Hariri-Ardebili *et al.* model predicts lower deflection than the test. It should be noted that the finite element mesh of the beam in Hariri-Ardebili *et al.* model is finer than Voyiadjis and Taqieddin (2009) model.

3.2 Experimental test on a gravity dam

The model of a typical concrete gravity dam scaled to 1:40 subjected to equivalent hydraulic lateral loads is analyzed applying incremental lateral loads using indirect displacement control algorithm (Carpenteri *et al.* 1992). The controlling parameter was selected to be crack mouth opening displacement (CMOD) of the notch and the adjusted incremental parameter due to the analysis was limited to 0.00002mm. Lateral hydraulic loads simulating the hydrostatic pressure on the upstream face are applied using four concentrated loads acting directly on the upstream through steel plates. Fig. 4(a) shows the geometry of the model and the percentage of lateral loads simulating the hydrostatic pressure. Totally 750 eight-node solid elements were used in finite

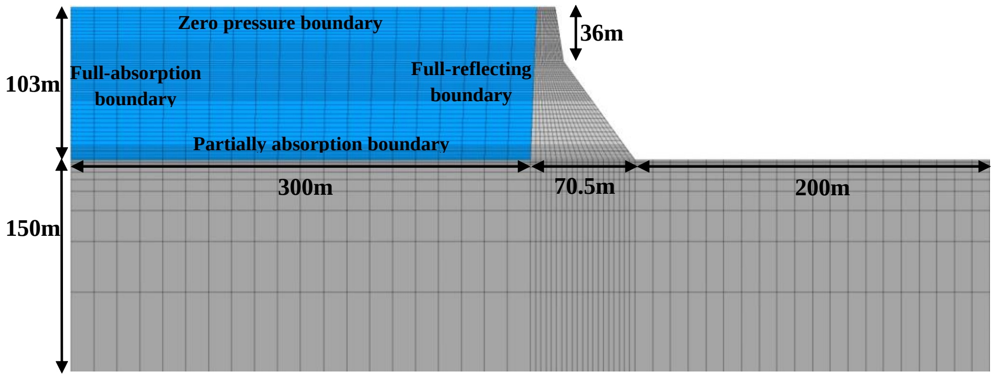

Fig. 5 Finite element model, dimensions and boundary conditions in dam-foundation-reservoir coupled system

element model of the scaled typical gravity dam. The material properties are as follow: E=35.7GPa, υ=0.1, f'_t=3.6MPa and G_f=184N/m. The crack band within the Gaussian points is assumed coaxial rotating crack. Load versus CMOD of the notch for the considered dam resulted from experimental test (Carpenteri *et al.* 1992) and the finite element model is depicted in Fig. 4(b). As seen, the theoretical results are in good agreement with those obtained from experimental test.

4. Finite element model of case study

In order to investigate the ability of the proposed method in dynamic analysis of mass concrete structures, Koyna gravity dam in India was selected as case study. This dam is one of a few concrete dams that have experienced a destructive earthquake. The finite element model of dam-foundation-reservoir coupled system is shown in Fig. 5. In this model, 3D eight-node solid elements were used for modeling the dam body and foundation rock and the fluid elements were used for simulation of the reservoir water. Only stiffness of the foundation was considered in total coupled equation of motion and the far-end boundaries of massless foundation were restricted in all translational directions. Fluid and solid elements are in interaction with each other at interface of dam-reservoir and also reservoir-foundation. Appropriate wave reflection coefficient was assumed in reservoir-foundation interface in order to modeling the bottom sediment effect. Far-end boundary of the reservoir was modeled in a way that absorbs all outgoing waves, while zero pressure boundary condition was applied at reservoir free surface. Detailed fluid-structure coupled equations and the mathematical representation of the fluid boundary conditions are summarized in Appendix (1).

Applied loads on the coupled system are dam body self-weight, hydrostatic pressure and seismic load (Hariri-Ardebili and Mirzabozorg 2012). The system was excited at foundation boundaries and Newmark-β time integration method was utilized to solve the coupled problem of dam-reservoir-foundation model. Moreover, structural damping was taken to be 5% of critical damping in both linear and nonlinear cases. Material properties of mass concrete and the foundation rock are as follow; E_c and υ_c are 31.03MPa and 0.2 in static condition (Chopra and Chakrabarti 1973), and 35.68MPa and 0.14 in dynamic condition, respectively. f'_t and f'_c are

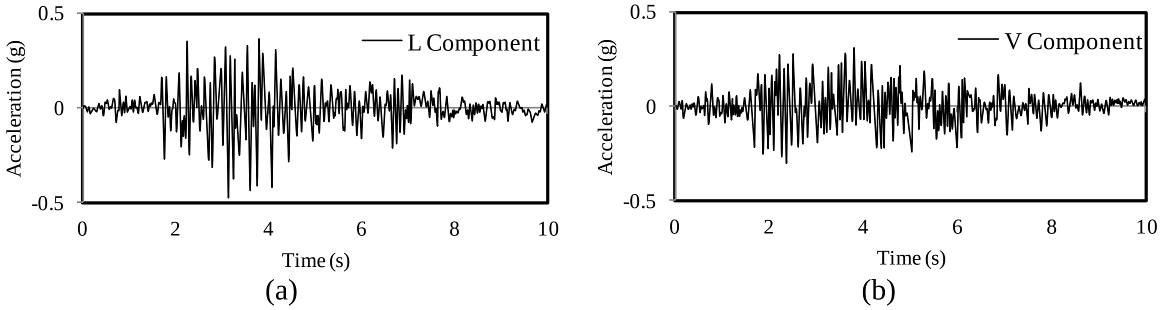

Fig. 6 The Koyna earthquake accelerogram record: (a) longitudinal component, (b) vertical component

2.4MPa and 24MPa in static condition (Guanglun *et al.* 2000), and 3.6MPa and 36MPa in dynamic condition, respectively. It is noteworthy that the material properties in dynamic condition were calculated based on USACE (2007) and FEMA (1999) recommendation considering the rate dependence of the mechanical and strength properties of mass concrete. Density of mass concrete is 2643kg/m^3 and the fracture energy is 300N/m. In addition modulus of elasticity and Poisson's ratio of rock were assumed to be 31MPa and 0.33, respectively. The acceleration time-histories of Koyna ground motion are shown in Fig. 6.

5. Results

5.1 Considering fracture energy

In this section, application of the proposed smeared crack model is investigated for the problem of fluid-structure interaction considering the fracture energy effects. Three types of nonlinear models and a linear model (as a reference one) were prepared. The geometry of dam, finite element model, material properties and the sequence of loading are the same in all models. The nonlinear models are different only in the values of the shear transfer coefficients. These three models are named as NL1, NL2 and NL3 and defined as follow:

• NL1: Constant values are assumed for shear transfer coefficients; 0.1 in open crack condition and 0.9 in closed crack condition. It shows the state of the crack in which the crack face is completely rough in closed and completely smooth in open condition.

• NL2: Constant values are assumed for shear transfer coefficients; 0.3 in open crack condition and 0.7 in closed crack condition. It shows the state of the crack in which the crack face is relatively rough in closed and relatively smooth in open condition.

• NL3: Variable values are considered for shear transfer coefficients in open and closed conditions which are updated in each load step of the analysis.

Fig. 7 represents time-history of crest displacement in stream direction for linear and three nonlinear models. As seen, all nonlinear models have almost the same behavior up to t=4.3s. The first model which is failed under the seismic loads is NL3 and the last one is NL1. It shows that using constant shear transfer coefficients for concrete behavior instead of variable coefficient overestimates the strength and stability of the dam and can leads to mis-interpretation of the results in dam safety related projects. Fig. 8 shows the crack profile in dam body under the seismic loads at different times and also final crack profile of Koyna Dam at failure time corresponding to large

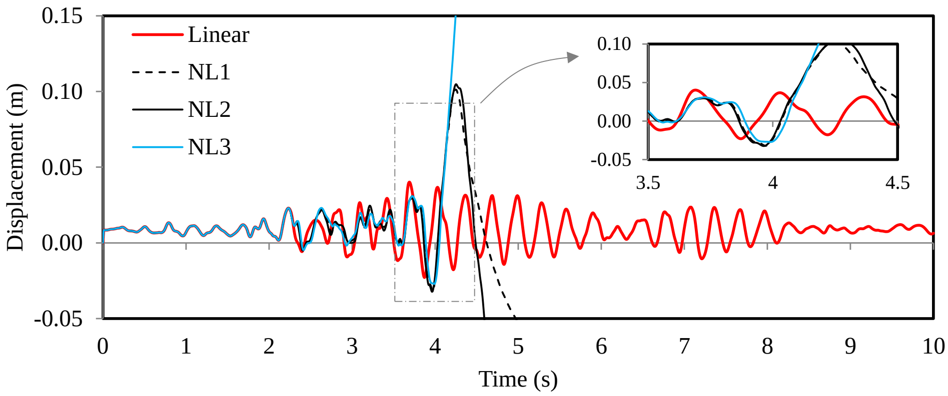

Fig. 7 Time-history of the crest displacement in stream direction; considering fracture energy

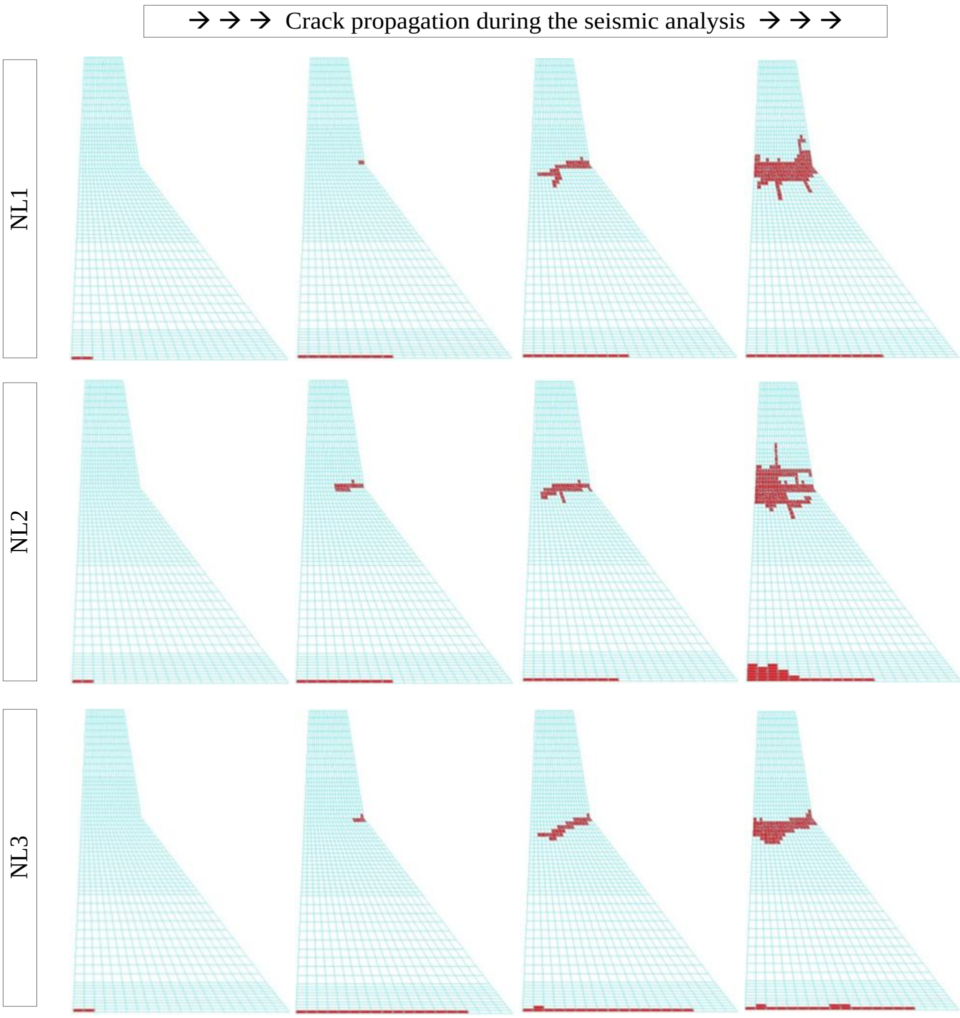

Fig. 8 Crack propagation in dam body and the final crack profile at failure time; considering fracture energy

drift as shown in Fig. 7. As it is clear, in all models cracking starts in heel of dam at dam-foundation interface while final cracking and failure of dam is due to continuous cracking in neck area which connects upstream and downstream of dam together. Using variable shear transfer coefficient leads to less diffusion of the cracked area in neck which is more real based on the observed crack profiles from shake table test. Also comparing NL1 and NL2 models shows that using 0.1 for open cracks and 0.9 for closed cracks leads to closer behavior to those obtained from variable shear transfer coefficients.

5.2 Neglecting fracture energy

Fig. 9 shows time-history of the crest displacement for linear and nonlinear models neglecting fracture energy effects. Although variable shear transfer coefficient model fails earlier than the others, there are no meaningful differences between three models (variable and constant shear transfer coefficients). It can be concluded that neglecting fracture energy effect leads to almost the same behavior in all nonlinear models in crack analysis of gravity dams. It means that, neglecting fracture energy effect covers the effects of the shear transfer coefficient. Fig. 10 shows the propagation of crack profile for nonlinear models neglecting fracture energy effects. Cracking starts at heel of dam in all models and propagate toward downstream. In addition, crack appears at the point of slope discontinuity on the downstream face and extends through the width of the neck toward upstream. The final crack profiles are close together while using variable shear transfer coefficient leads to lower cracked area than two other models. Neglecting fracture energy extends cracking through the entire dam-foundation interface at the final crack profile. Total stability of the coupled system due to base movement and overturning of the dam body should be checked in this condition.

6. Discussion

6.1 Input ground motion effect

The presented results in the previous section are subjective to Koyna earthquake. In order to generalizing the findings of the present research over the other earthquake scenarios, four other

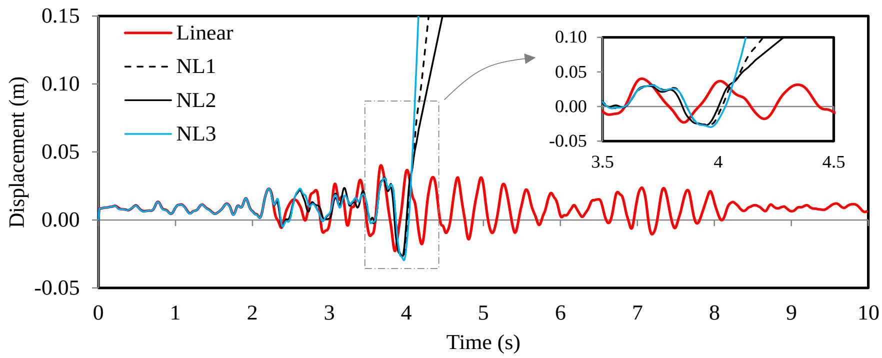

Fig. 9 Time-history of the crest displacement in stream direction; neglecting fracture energy

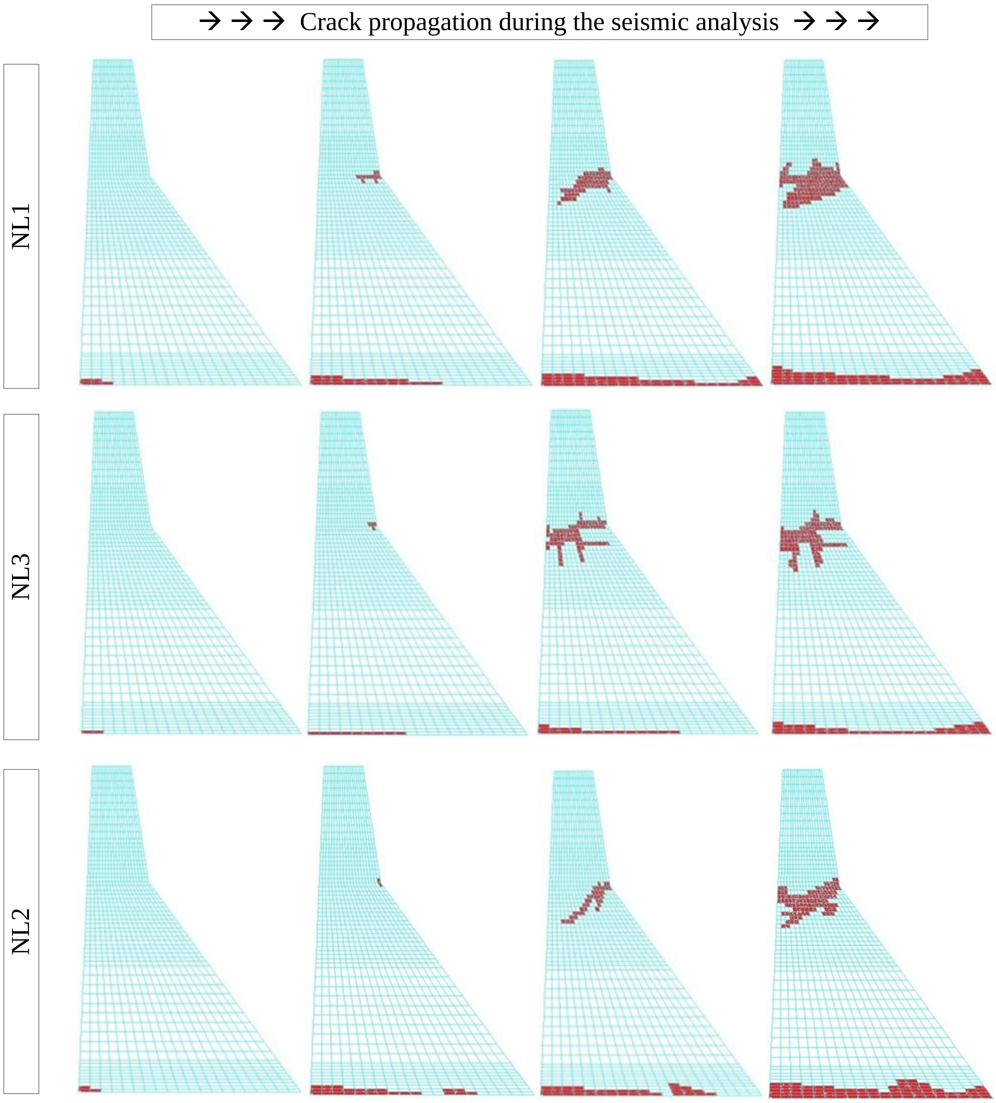

Fig. 10 Crack propagation in dam body and the final crack profile at failure time; neglecting fracture energy

ground motions with different fault mechanisms were selected (Hariri-Ardebili and Mirzabozorg 2012). Considering that there was no accessible design response spectrum for the Koyna Dam, the smoothed horizontal and vertical acceleration response spectrums of the Koyna ground motion were used as target spectrums as shown in Fig. 11(a). PEER ground motion database (2010) was used for selection of the other ground motions which matches reasonably with the target spectrum based on the general site characteristics of Koyna Dam. Fundamental characteristics of these ground motions are summarized in Table 1. Also the response spectrums of these four scaled ground motions are compared with the target one in Fig. 11(b). It should be noted that the effects of the spatial varying ground motions are not considered in the present study (Mirzabozorg *et al.* 2012).

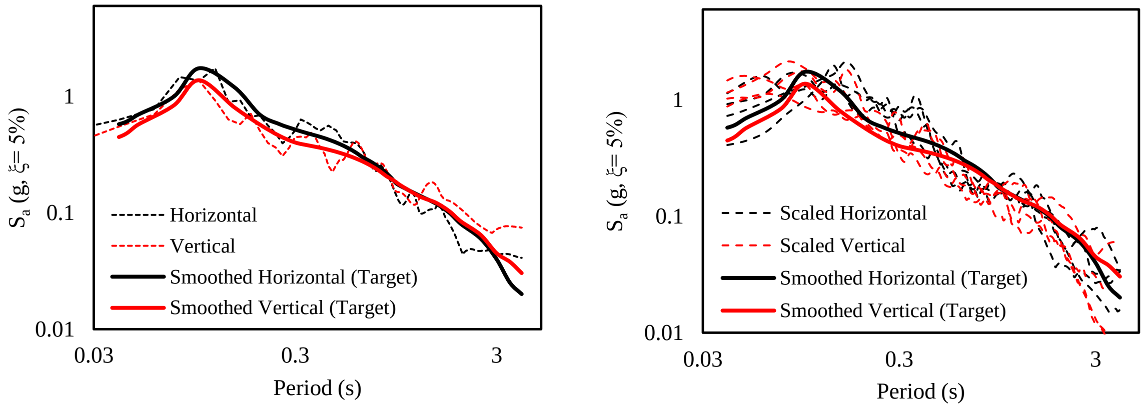

(a) (b)

Fig. 11 (a) Original and smoothed target response spectrums of Koyna earthquake; (b) Scaled response spectrums of the selected ground motions

Table 1 Characteristics of the selected ground motions

Abbreviation	Event	Year	Station	M*	Fault Mechanism	R_{rup}** (km)	V_{S30}*** (m/s)	$D_{5\text{-}95}$† (s)
MOH	Morgan Hill	1984	Gilroy- Gavilan Coll.	6.19	Strike-Slip	14.8	729	8.6
SAF	San Fernando	1971	Lake Hughes # 9	6.61	Reverse	22.6	670	9.4
LOP	Loma Prieta	1989	UCSC	6.93	Reverse-Oblique	18.5	714	8.5
IRP	Irpinia, Italy	1980	Brienza	6.90	Normal	22.6	500	9.7

* moment magnitude
** closest distance to rupture plane
*** average shear wave velocity of top 30 meters of the site
† significant duration of the record (the time needed to build up between 5% and 95% of the total Arias intensity)

Effect of the fracture energy is investigated only for the model with variable shear transfer coefficient (NL3) because this one is the most accurate model over the three nonlinear models. Fig. 12 shows the final crack profile of the dam body under the four scaled ground motions with/without the fracture energy effect. As it is clear, in all cases neglecting the fracture energy effect leads to more cracked elements within the dam body. Cracking starts at the heel of the dam when the effects of the fracture energy is considered and propagates toward downstream. There is no entire cracking at the dam base in this condition. Neglecting the fracture energy effect leads to more cracked element at the dam-foundation interface as well as complete base for IRP ground motion. In addition, the numbers of cracked elements at the neck area increase when the fracture energy effect is neglected. It should be noted that the effective duration of the ground motions is almost the same in all cases and so the final crack profile is not highly sensitive to input ground motion duration (Hariri-Ardebili and Mirzabozorg 2013).

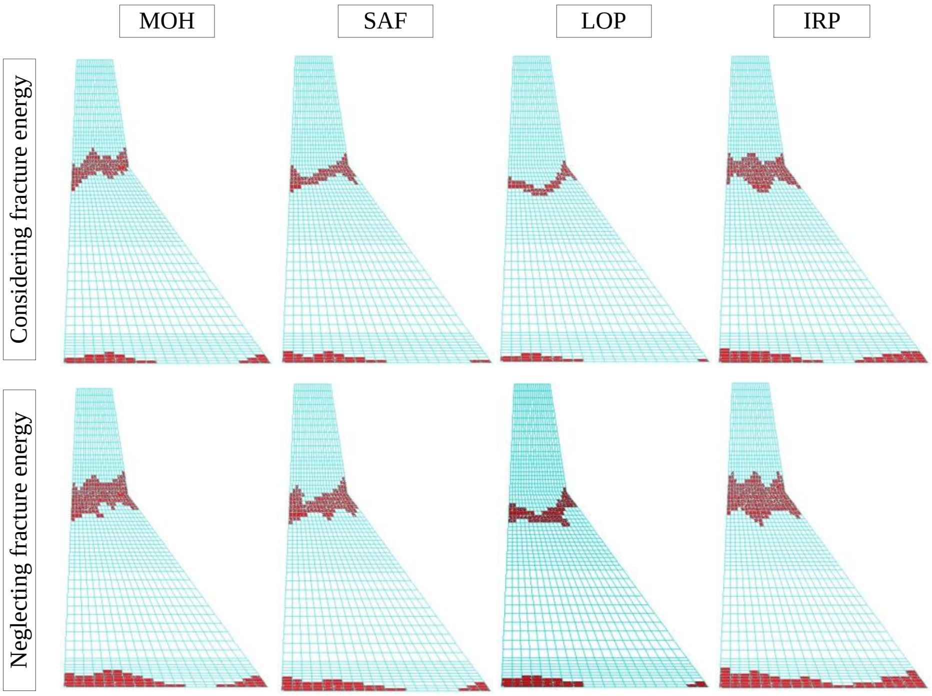

Fig. 12 Comparison of the final crack profile for different ground motion scenarios; variable shear transfer coefficient model

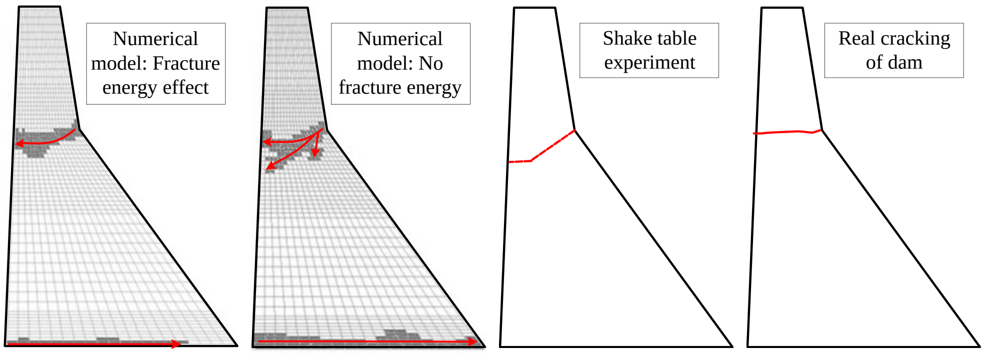

Fig. 13 Comparison of the final crack profile in dam body resulted from numerical models, experimental test and the real dam cracking

6.2 Experimental test and model comparison

Analyzing the results of the previous section reveals that the neck area and also dam-foundation interface near the heel are most crack-prone areas. Fig. 13 compares the final crack profile of the dam based on variable shear transfer coefficient under Koyna earthquake with real dam cracking and also experimental test. As seen, neglecting fracture energy leads to start of the cracking at the slope-change-point in downstream of the neck and propagation of cracks toward upstream face and lower parts, while considering its effects leads to propagation of cracks along the specific line

Table 2 Summary of the finite element models characteristics for crack analysis of Koyna Dam

Model (year)	Characteristics	Description/Comparison
Omidi *et al*. (2013)	Material properties	f'_t=2.9MPa, f_c=24.1MPa, G_t=200N/m, G_c=20000N/m, C_0=1440m/s, α=0.85
	FSI model	Eulerian-Lagrangian approach
	Foundation model	Rigid foundation
	Constitutive model	Plastic-damage model in 3D context
	Damping	Constant and damage-dependent damping mechanism
	Load combination	Self-weight + hydrostatic pressures + Seismic loading
Guanglun *et al*. (2000)	Material properties	E_c=31.6GPa, f'_t=2.46MPa, f_c=24.6MPa, υ=0.2, G_f=250N/m, γ_c=26.4kN/m^3
	FSI model	Neglected
	Foundation model	Rigid foundation
	Constitutive model	Nonlinear fracture mechanics
	Damping	Stiffness proportional damping, ξ=5%
	Load combination	Self-weight + hydrostatic pressures + Seismic loading
Calayir and Karaton (2005)	Material properties	E_c=31.027GPa, f'_t=1.5MPa, $(f'_t)_{dyn}$=1.8MPa, υ=0.2, G_f=150N/m, $(G_f)_{dyn}$=180N/m, ρ_c=2643kg/m^3, κ=2070MPa
	FSI model	Lagrangian-Lagrangian approach
	Foundation model	Rigid foundation
	Constitutive model	Coaxial rotating crack model with biaxial failure envelope
	Damping	Stiffness proportional damping, ξ=5%
	Load combination	Self-weight + hydrostatic pressures + Seismic loading
Calayir and Karaton (2005)	Material properties	E_c=31.027GPa, f'_t=2.0MPa, υ=0.2, G_f=200N/m, ρ_c=2643kg/m^3, κ=2070MPa
	FSI model	Lagrangian-Lagrangian approach
	Foundation model	Rigid foundation
	Constitutive model	Orthotropic damage model
	Damping	Stiffness proportional damping, ξ=5%
	Load combination	Self-weight + hydrostatic pressures + Seismic loading
Pan *et al.* (2011)	Material properties	E_c=31GPa, f'_t=2.9MPa, f_c=28.9MPa, υ=0.2, G_f=250N/m
	FSI model	Westergaard added mass
	Foundation model	Rigid foundation
	Constitutive model	plastic-damage model + Drucker-Prager elasto-plastic model
	Damping	Rayleigh damping, ξ=5%
	Load combination	Self-weight + hydrostatic pressures + Seismic loading

from downstream neck to upstream face. Also neglecting fracture energy effects leads to complete cracking of the base in vicinity of the foundation.

Fig. 13 shows shaking table test on the 1:150 scaled model of Koyna Dam (performed at the University of California, Berkeley) and resulted cracks at the elevation of the downstream slope-change (Hall 1988). Also this figure shows the real crack profile in Koyna Dam as reported by Saini and Krishna (1974). Comparing the real crack profile, the experimental results and the proposed numerical model reveals that this model is able to capture the crack propagation in mass concrete structures with the good accuracy.

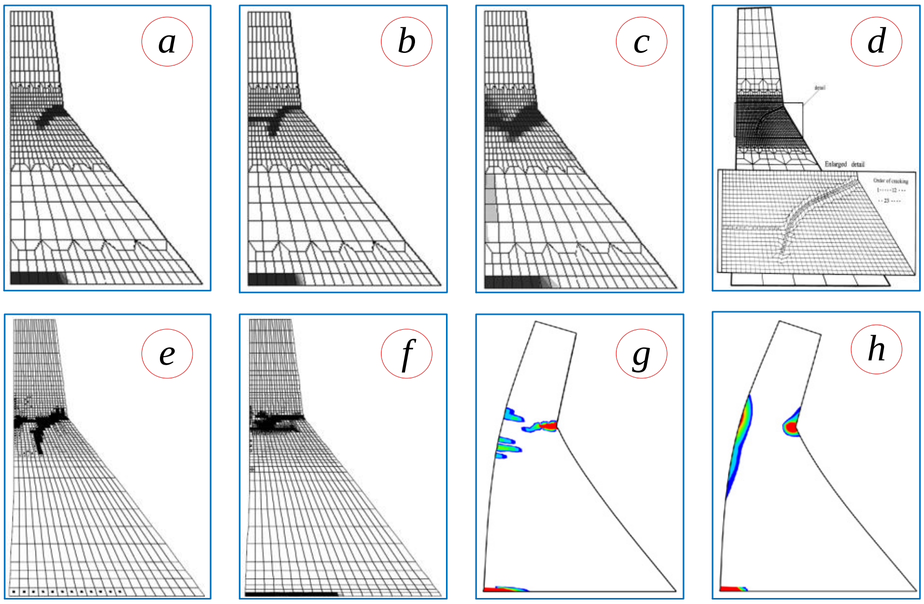

Fig. 14 Comparison of the final crack profile of Koyna Dam subjected to 1967 Koyna earthquake obtained by different researchers

6.3 Comparison among various numerical models

In the present subsection, the final crack profile of Koyna Dam under Koyna ground motion is compared with the results obtained by the other researchers. First the basic assumptions in each one is described and then the similarities and differences between then will be discussed. Table 2 summarizes the basic assumptions, material properties and the numerical modeling in each case.

Omidi *et al.* (2013) studied the behavior of Koyna Dam based on damage plasticity model. They considered two damping mechanism models, i.e., constant and damage dependent. They found that in the case of the constant damping, the diffused damage penetrates more at the slope change on the downstream face (Fig. 14(a)) while in the case of damage-dependent damping the whole neck area cracks (Fig. 14(b)). In the case of using reduced material properties (f'_t=1.5MPa and G_f=150N/m) the resulted crack profile is shown in Fig. 14(c) which leads to more damage. Guanglun *et al.* (2000) studied 2D nonlinear seismic fracture behavior of Koyna Dam. They reported that crack appears initially at the point of slope discontinuity on the downstream face and extends about two-thirds through the width of the neck, and then upstream crack starts propagating horizontally to reach the downstream crack (Fig. 14(d)). Calayir and Karaton (2005) studied the seismic behavior of Koyna Dam using coaxial rotating crack model. They found that cracked elements are extended over the entire the neck and also about 60% of the base of the dam. The cracks at the downstream face are initially horizontal and propagate deeper inside of the dam. At the same time, previously initiated cracks in the heel of the dam propagate from the heel to the toe as shown in Fig. 14(e). Also Calayir and Karaton (2005) investigated Koyna Dam behavior based on orthotropic damage model for mass concrete. Due to the infinite rigidity of the foundation, crack propagates at the base of the dam. The final crack pattern at the neck area in this case is different from their previous study (Fig. 14(f)). Pan *et al.* (2011) investigated the crack behavior of

Koyna Dam using damage plastic (Fig. 14(g)) and Drucker-Prager elasto-plastic (Fig. 14(h)) models. They found that cracking starts from downstream face at the point of slope discontinuity and propagates towards upstream. Also when the dam oscillates to the downstream direction and reaches the first large downstream displacement, cracks begin to initialize near the middle of the upstream face.

7. Conclusions

A coaxial rotating smeared crack model was introduced for nonlinear behavior of mass concrete in three-dimensional space which was able to utilize variable shear transfer coefficient, an advanced three-parameter yield criterion, and simulation of cracking process in concrete with high accuracy. Finite element model of Koyna gravity dam-reservoir-foundation system was provided in order to investigation of the nonlinear dynamic behavior of large concrete specimens considering fluid-structure-interaction. The system was excited using Koyna ground motion recorded during Koyna earthquake. In addition, four other ground motions with different mechanisms were applied to the coupled system in order to generalizing the results. The results were compared for constant and variable shear transfer coefficients considering and neglecting the fracture energy effects.

It was found that the proposed model is capable of crack analysis of large concrete specimens under the high hydrostatic pressure. Generally shear transfer coefficient affects the results of the dynamic analysis while fracture energy effects are considered. Considering fracture energy effects lead to creation of crack profiles with less diffusion especially in neck area of dam which is more close to reality. It was observed that neglecting fracture energy effects lead to failure of models (with different shear transfer coefficients) almost in the same time. Considering the fracture energy leads to failure of the models in various times. Finally it was concluded that the proposed model can be used for seismic crack analysis of concrete gravity dams considering the effects of fluid-structure interaction.

Acknowledgements

The authors would like to thank anonymous reviewers for their useful comments which have greatly improved the manuscript.

References

Al-Rub, R.K.A. and Kim, S.M. (2010), “Computational applications of a coupled plasticity-damage constitutive model for simulating plain concrete fracture”, *Eng Fract Mech*, **77**(10), 1577-1603.

Ayari, M.L. and Saouma, V.E. (1990), “A fracture mechanics based seismic analysis of concrete gravity dams”, *Eng Fract Mech*, **35**, 587-598.

Babu, R., Benipal, G.S. and Singh, A.K. (2005), “Constitutive modeling of concrete: An overview”, *Asian J. Civil Eng.*, **6**(4), 211-246.

Bazant, Z.P. (2002), “Concrete fracture models: testing and practice”, *Eng Fract Mech*, **69**, 165-205.

Bhattacharjee, S.S. and Leger, P. (1994), “Application of NLFM models to predict cracking in concrete gravity dams”, *Struct. Eng.*, **120**(4), 1255-1271.

Bigoni, D. and Piccolroaz, A. (2004), "Yield criteria for quasi brittle and frictional materials", *Solid. Struct.*, **41**, 2855-2878.

Briihwiler, E. and Wittmann, F.H. (1990), "Failure of dam concrete subjected to seismic loading conditions", *Eng. Fract. Mech.*, **35**, 565-571.

Broujerdian, V. and Kazemi, M.T. (2010), "Smeared rotating crack model for reinforced concrete membrane elements", *ACI Struct. J.*, **107**(4), 411-418.

Calayir, Y. and Karaton, M. (2005), "A continuum damage concrete model for earthquake analysis of concrete gravity dam-reservoir systems", *Soil Dyn. Earthq. Eng.*, **25**(11), 857-869.

Calayir, Y. and Karaton, M. (2005), "Seismic fracture analysis of concrete gravity dams including dam-reservoir interaction", *Comput. Struct.*, **83**(19-20), 1595-1606.

Carpinteri, A., Valente, S.V., Ferrara, G. and Imperato, L. (1992), "Experimental and numerical fracture modeling of a gravity dam", *Proceedings of the 1st International Conference on Fracture Mechanics of Concrete Structures*, Breckenridge, Colorado.

Chopra, A.K. and Chakrabarti, P. (1973), "The Koyna earthquake and the damage to Koyna dam", *Bul. Seismol. Soc. Am.*, **63**, 381-397.

Cicekli, U., Voyiadjis, G.Z. and Abu Al-Rub, R.K. (2007), "A plasticity and anisotropic damage model for plain concrete", *Int. J. Plasticity*, **23**, 1874-1900.

Duan, K., Hu, X. and Wittmann, F.H. (2007), "Size effect on specific fracture energy of concrete", *Eng. Fract. Mech.*, **74**(102), 87-96.

Duan, K., Hu, X. and Wittmann, F.H. (2003), "Boundary effect on concrete fracture induced by non-constant fracture energy distribution", *Eng. Fract. Mech.*, **70**(16), 2257-2268.

Einsfeld, R.A. and Velasco, M.S.L. (2006), "Measurement of the ratio G_F/G_f for numerical analysis of concrete structures", *Latin Am. J. Solid. Struct.*, **3**, 361-376.

Federal Energy Regulatory Commission (FERC). (1999), "Engineering guidelines for the evaluation of hydropower projects, Chapter 11: Arch Dams", Washington, USA.

Ghaemian, M. and Ghobarah, A, (1999), "Nonlinear seismic response of concrete gravity dams with dam-reservoir interaction", *Eng. Struct.*, **21**, 306-315.

Ghrib, F. and Tinawi, R. (1995), "Nonlinear behavior of concrete dams using damage mechanics", *Eng. Mech.*, ASCE, **121**(4), 513-526.

Grassl, P. and Jirásek, M. (2006), "Damage-plastic model for concrete failure", *Int. J. Solid. Struct.*, **43**(22-23), 7166-7196.

Guanglun, W., Pekau, O.A., Chuhan, Z. and Shaomin, W. (2000), "Seismic fracture analysis of concrete gravity dams based on nonlinear fracture mechanics", *Eng. Fract. Mech.*, **65**(1), 67-87.

Hal, J.F. (1988), "The dynamic and earthquake behavior of experimental behavior and observational evidence", *Soil Dyn. Earthq. Eng.*, **7**(2), 58-121.

Hariri-Ardebili, M.A. and Mirzabozorg, H. (2013), "A comparative study of the seismic stability of coupled arch dam-foundation-reservoir systems using infinite elements and viscous boundary models", *J. Struct. Stabil. Dyn.*, **13**(6), DOI: 10.1142/S0219455413500326.

Hariri-Ardebili, M.A., Mirzabozorg, H. and Kianoush, M.R. (2013), "Seismic analysis of high arch dams considering contraction-peripheral joints coupled effects", *Centr. Eur. J. Eng.*, **3**(3), 549-564.

Hariri-Ardebili, M.A., Mirzabozorg, H. and Ghasemi, A. (2013), "Strain-based seismic failure evaluation of coupled dam-reservoir-foundation system", *Coupl. Syst. Mech.*, **2**(1), 85-110.

Hariri-Ardebili, M.A. and Mirzabozorg, H. (2012), "Seismic performance evaluation and analysis of major arch dams considering material and joint nonlinearity effects", *ISRN Civil Eng.*, Article ID 681350.

Hariri-Ardebili, M.A. and Mirzabozorg, H. (2012), "Effects of near-fault ground motions in seismic performance evaluation of a symmetry arch dam", *Soil Mech. Found. Eng.*, **49**(5), 192-199.

Heinrich, C. and Waasy, A.M. (2012), "Investigation of progressive damage and fracture in laminated composites using the smeared crack approach", *Proceedings of the 53rd AIAA/ASME/ASCE/AHS/ASC Structures, Structural Dynamics and Materials Conference*, Honolulu, Hawaii.

Hu, X. and Duan, K. (2004), "Influence of fracture process zone height on fracture energy of concrete", *Cement Concrete Res.*, **34**(8), 1321-1330.

Labadi, Y. and Hannachi, N.E. (2005), "Numerical simulation of brittle damage in concrete", *Int. J. Strength* . **37**(3), 268-281.

Lohrasbi, A.R. and Attarnejad, R. (2008), "Crack growth in concrete gravity dams based on discrete crack method", *Am J. Eng. Appl. Sci*, **1**(4), 318-323.

Malvar, L.J. and Fourney, M.E. (1990), "A three dimensional application of the smeared crack approach", *Eng. Fract. Mech.*, **35**(1-3), 251-260.

Malvar, L.J. and Warren, G.E. (1988), "Fracture energy for three-point-bend tests on single-edge-notched beams", *Exp. Mech*, **45**, 266-272.

Menetrey, P.H. and Willam, K.J. (1995), "Tri-axial failure criterion for concrete and its generalization", *Int. J. ACI Struct*, **92**, 311-318.

Mirzabozorg, H., Akbari, M. and Hariri-Ardebili, M.A. (2012), "Wave passage and incoherency effects on seismic response of high arch dams", *Earthq. Eng Eng Vib*, **11**(4), 567-578.

Mirzabozorg, H. and Ghaemian, M. (2005), "Nonlinear behavior of mass concrete in three-dimensional problems using smeared crack approach", *Earthq Eng Struct Dyn*, **34**, 247-269.

Mirzabozorg, H., Ghaemian, M. and Kianoush, R. (2004), "Damage mechanics approach in seismic analysis of concrete gravity dams including dam-reservoir interaction", *Eur Earthqe Eng*, **XVIII**(3), 17-24.

Mirzabozorg, H., Khaloo, A.R., Ghaemian, M. and Jalalzadeh, B. (2007), "Non-uniform cracking in smeared crack approach for seismic analysis of concrete dams in 3D space", *Earthq Eng. Eng. Seism*., **2**, 48-57.

Moslera, J. and Meschke, G. (2004), "Computational failure mechanics embedded crack vs. smeared crack models: a comparison of element wise discontinuous crack path approaches with emphasis on mesh bias", *Comput Meth. App. Mech. Eng.*, **193**(30-32), 3351-3375.

Omidi, O., Valliappan, S. and Lotfi, V. (2013), "Seismic cracking of concrete gravity dams by plastic-damage model using different damping mechanisms", *Finite Elem. Anal. Des.*, **63**, 80-97.

Pan, J., Zhang, C., Xu, Y. and Jin, F. (2011), "A comparative study of the different procedures for seismic cracking analysis of concrete dams", *Soil Dyn. Earthq. Eng.*, **31**(11), 1594-1606.

PEER ground motion database (2010), http://peer.berkeley.edu/peer_ground_motion_database, Beta version, University of California, Berkeley, CA, USA.

Phama, H.B., Al-Mahaidia, R. and Saouma, V. (2006), "Modeling of CFRP-concrete bond using smeared and discrete cracks", *Proceedings of the 13th International Conference on Composite Structures*, **75**(1-4), 145-150.

RILEM TC 50-FMC (1985), "Determination of fracture energy of mortar and concrete by means of three-point bend tests on notched beams", *Mater. Struct.*, **18**(106), 285-290.

Saini, S.S. and Krishna, J. (1974), "Overturning of top profile of the Koyna dam during severe ground motion", *Earthq. Eng. Struct. Dyn.*, **2**(3), 207-217.

Saouma, V.E. and Morris, D. (1998), "Application of fracture mechanics to concrete dams: a detailed case study". *Dam Eng.*, **9**(4), 321-344.

Saouma, V.E. and Milner, D. (1996), "On why fracture mechanics should be used in dam safety evaluation", *Dam Eng.*, 7(3), 215-231.

Suryanto, B., Nagai, K. and Maekawa, K. (2010), "Smeared-crack modeling of R/ECC membranes incorporating an explicit shear transfer model", *J. Adv. Concrete Tech.*, **8**(3), 315-326.

US Army Corps of Engineers (USACE) (2007), "EM 1110-2-6053: Earthquake design and evaluation of concrete hydraulic structures", Washington, USA.

Voyiadjis, G.Z., Taqieddin, Z.N. and Kattan, P.I. (2009), "Theoretical formulation of a coupled elastic-plastic anisotropic damage model for concrete using the strain energy equivalence concept", *Int. J. Damage Mech.*, **18**, 603-638.

Voyiadjis, G.Z. and Taqieddin, Z.N. (2009), "Elastic plastic and damage model for concrete materials, Part I: Theoretical formulation", *Int. J. Struct. Change. Solid. – Mech. Appl.*, **1**(1), 31-59.

Weihe, S., Kröplin, B. and De Borst. R. (1998), "Classification of smeared crack models based on material and structural properties", *Int. J. Solid. Struct.*, **35**(12), 1289-1308.

Xue, X. and Yang, X. (2013), "A damage model for concrete under cyclic actions", *Int. J. Damage Mech.*,

DOI: 10.1177/1056789513487084.
Yu, R.C., Ruiz, G. and Chaves, E.W.V. (2008), "A comparative study between discrete and continuum models to simulate concrete fracture", *Eng. Fract. Mech.*, **75**, 117-127.

Appendix 1

Hydrodynamic pressure distribution in reservoir is governed by pressure wave equation. Assuming that water is compressible and neglecting viscosity, small-amplitude irrotational motion of water is governed as: (Mirzabozorg *et al.* 2012)

$$\nabla^2 P = \frac{1}{f(\rho_F)} \frac{\partial^2 P}{\partial t^2} \tag{a-1}$$

where $f(\rho_F)$ can be defined as

$$f(\rho_F) = \begin{cases} C_0^2 & when \quad \rho_F \geq -P_v / C_0^2 \\ -P_v / \rho_F & when \quad \rho_F \leq -P_v / C_0^2 \end{cases} \tag{a-2}$$

where P is hydrodynamic pressure, C_0 is velocity of pressure wave in water, ρ_F is density of fluid and P_v is vapor pressure of water. The relation between the pressure and density is constant for non-cavitating fluids such that $P = C_0^2 \rho_F$ (present study). However, for a cavitating fluid, the pressure-density relationship takes the nonlinear form. Under dynamic excitation, condition at boundaries on dam-reservoir ($\partial\Gamma_{FSI}$), reservoir-foundation ($\partial\Gamma_{FRI}$), reservoir-far-end ($\partial\Gamma_{F\infty}$) and reservoir-free-surface ($\partial\Gamma_{F0}$) for a non-cavitating fluid are governed as (Fig. 15)

At fluid-structure interface, there must be no flow across the face because the concrete dams are impermeable (Hariri-Ardebili *et al.* 2013). In the following equation, superscript "*s*" refers to structure

$$\frac{\partial P}{\partial n} + \rho_F {a^s}_n = 0 \quad on \quad \partial\Gamma_{FSI} \tag{a-3}$$

where ${a^s}_n$ is normal acceleration of dam body on upstream face and n is normal vector on interface of dam-reservoir outwards the body. Reservoir-foundation boundary condition considering the bottom sediments can be written as

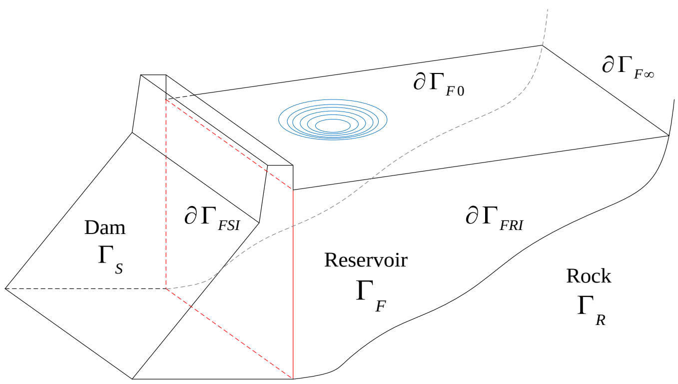

Fig. 15 Boundary conditions for dam-reservoir-foundation system

$$\frac{\partial P}{\partial n} + \rho_F a_n - q\frac{\partial P}{\partial t} = 0 \quad on \quad \partial\Gamma_{FRI} \tag{a-4}$$

where q is admittance coefficient and the relation between q and α (wave reflection coefficient at the reservoir bottom and sides) is expressed as

$$\alpha = \frac{1 - qC_0}{1 + qC_0} \tag{a-5}$$

In high reservoirs, surface waves are negligible and hydrodynamic pressure on free surface is set to be zero.

$$P = 0 \quad on \quad \partial\Gamma_{F0} \tag{a-6}$$

For modeling the far-end truncated boundary, viscous boundary condition is utilized to absorb completely the outgoing pressure waves given as:

$$\frac{\partial P}{\partial n} + \frac{1}{C_0}\frac{\partial P}{\partial t} = 0 \quad on \quad \partial\Gamma_{F\infty} \tag{a-7}$$

The coupled equations of the dam-foundation-reservoir take the form (Hariri-Ardebili *et al.*, 2013)

$$\begin{cases} [M]\{\ddot{U}\} + [C]\{\dot{U}\} + [K]\{U\} = \{f_1\} - [M]\{\ddot{U}_g\} + [Q]\{P\} = \{F_1\} + [Q]\{P\} \\ [G]\{\ddot{P}\} + [C']\{\dot{P}\} + [K']\{P\} = \{F\} - \rho_F [Q]^T \left(\{\ddot{U}\} + \{\ddot{U}_g\}\right) = \{F_2\} - \rho_F [Q]^T \{\ddot{U}\} \end{cases} \tag{a-8}$$

where [M], [C] and [K] are the mass, damping and stiffness matrices of the structure including the dam body and its foundation media and [G], [C'] and [K'] are representing the mass, damping and stiffness equivalent matrices of the reservoir, respectively. The matrix [Q] is the coupling matrix; {f_1} is the vector including both the body and the hydrostatic force; {P} and {U} are the vectors of hydrodynamic pressures and displacements, respectively and {$\ddot{U}_g$} is the ground acceleration vector. A detailed definition of matrices and vectors used in Eq. (a-8) has been provided in Hariri-Ardebili *et al.* (2013).